American Mineralogist, Volume 63, pages 40–46, 1978

Phase equilibria in fluid inclusions in ultramafic xenoliths

BARBARA W. MURCK, ROBERT C. BURRUSS AND LINCOLN S. HOLLISTER

Department of Geological and Geophysical Sciences
Princeton University, Princeton, New Jersey 08540

Abstract

Over 200 fluid inclusions in five dunite, peridotite, and pyroxenite xenoliths associated with basaltic rocks from Arizona, Hawaii, and Germany were examined using a petrographic microscope equipped for cooling to −140°C.

The temperatures of phase changes observed in individual fluid inclusions are interpreted according to published, experimentally determined phase equilibria as follows:

(1) Most inclusions contain nearly pure CO_2 and, in some cases, a small amount (on the order of 0.05 to 0.10 mole fraction) of SO_2, H_2S, or COS. Only one inclusion contains a possible aqueous phase.

(2) The CO_2 fluid densities range from 0.34 to 1.14 gm/cm³. Assuming a temperature of entrapment of 1200°C, this implies confining pressures of more than 10 kilobars at the time of entrapment of the densest inclusions.

The presence of glass linings on some of the inclusion walls suggests coexistence at depth of a CO_2-rich volatile phase with a melt phase at the time of entrapment of the two fluids in the host minerals. Compositions of the glass linings of two samples, Dreiser Wehier, Germany, and Red Hill, Arizona, most closely match high-alumina andesite and high-alumina basalt, respectively.

Introduction

Roedder (1965) identified ubiquitous, nearly pure liquid and gaseous CO_2 fluid inclusions, commonly containing glass, in dunitic, peridotitic, pyroxenitic, and gabbroic xenoliths from many localities throughout the world. He reported similar occurrences of CO_2-rich inclusions in basalts, eclogite xenoliths, and kimberlites. The present study is an extension of Roedder's work on xenoliths in basaltic rocks. Precise measurements were made of the temperatures of phase transitions within individual fluid inclusions in olivine and pyroxene in an attempt to identify any other components present in the CO_2-rich phase and to determine the bulk density of the CO_2 fluid. Compositions of the glass linings of fluid inclusions in the samples were obtained by microprobe analysis.

Analytical procedure

We examined five samples of dunitic, pyroxenitic, and peridotitic xenoliths associated with basalt. Table 1 is a brief description of the samples, their locations, and their sources. Samples were cut to a thickness of 0.25 mm and doubly polished, then examined on a petrographic microscope equipped with a CHAIX-MECA heating and cooling stage (Poty *et al.*, 1976). The temperatures of phase transitions in each inclusion were observed over the interval −140° to +40°C. These observations were compared with literature data on low-temperature phase equilibria for possible gas species associated with basaltic magmas. Possible species are listed in Table 2 and were selected in accordance with the calculations of Gerlach and Nordlie (1975) and the observations of Rama *et al.* (1965) and Funkhouser and Naughton (1968). Low-temperature phase equilibria for the systems CO_2–CH_4, CO_2–H_2O, and CO_2–CH_4–H_2O were summarized by Hollister and Burruss (1976). Additional data on CO_2 mixtures with SO_2, H_2S, and CO are also available in Cummings (1931), Sobocinski and Kurata (1959), and Christiansen (1974), respectively.

The heating rate for homogenization measurements was 1.0°C/min. For melting temperatures it was 0.3°C/min. Reproducibility of measurements is approximately ±0.2 degrees. The final melting tem-

0003-004X/78/0102-0040$02.00

Table 1. Descriptions, locations, and sources of samples

ER-63-33
Locality: Kapulehu lava flow, 1801, Hualalai, Hawaii, U.S.A.
Source: E. Ingerson via D. Gottfried via E. Roedder
Description: angular, 4-8 cm dunite xenolith in vesicular basalt; olivine + clinopyroxene + orthopyroxene + spinel

OB-120
Locality: Dreiser Weiher, near Dreis, 8 km west of Kelberg and 8 km north of Daun, Eifel, Germany
Source: Princeton University petrology collection (H.H. Hess)
Description: same as sample ER-63-120 (Roedder, 1965) olivine, clinopyroxene, orthopyroxene, biotite in an olivine-rich peridotite xenolith, encased in vesicular basaltic glass

OB-140
(no fluid inclusions with measurable phase equilibria were found in this sample)
Locality: Gila County, Arizona, U.S.A. (probably Rice Station)
Source: Princeton University petrology collection (Ralph Cannon via H.H. Hess)
Description: same as sample ER-63-119 and 119a (Roedder, 1965)
very pristine olivine, some clinopyroxene and orthopyroxene; an olivine-rich peridotite xenolith from a bomb of vesicular basalt

SLC
Locality: Salt Lake Crater, Oahu, Hawaii, U.S.A.
Source: Robert Hargraves
Description: pyroxenite xenolith from basaltic tuff

RH
Locality: Red Hill, north of Williams, Arizona, U.S.A.
Source: Princeton University petrology collection (probably H.H. Hess)
Description: pyroxenite nodule

perature (invariant point) is defined as the disappearance of solid in the presence of liquid and vapor.

Results

Variations in sizes and morphologies of some representative inclusions are illustrated in Figure 1. The morphologies of the inclusions may be grouped into the following categories: semi-faceted; faceted (negative crystal); ovoid; spherical; cylindrical; irregular; and dendritic. The inclusions occur on fracture surfaces, associated with grain boundaries; in groups or on planes defined by crystallographic or twin directions; in random groups; and in isolation. Crystalline solids occur within some inclusions, and glass-rimmed inclusions are present in all five samples. Physical evidence of some leakage of contents, though rare, was noted (Fig. 1).

All inclusions containing a fluid phase are CO_2-rich. The apparent paucity of H_2O in these samples is noteworthy: only one inclusion contained an immiscible phase interpreted as a possible aqueous solution. The following data and discussion refer to miscible components in the CO_2-rich fluids. Observed homogenization temperatures, melting temperatures, and calculated densities for each inclusion as well as data on sizes, morphologies, modes of occurrence, and number of phases present at room temperature, are reported in Murck (1976). Representative data are shown in Table 3. Fluid inclusions with measurable phase equilibria were found in 4 of the 5 samples considered (OB-120, RH, SLC, ER-63-33).

All final melting temperatures are shown as a histogram in Figure 2. The invariant temperature at which pure CO_2 solid, liquid, and vapor are in equilibrium is $-56.6C°$ (Newitt *et al.*, 1956). Fifty-nine of 73 melting temperatures are $-56.6°C \pm 0.4°C$, the range which encompasses our estimated maximum observational error. Of the 14 temperatures which fall outside this range, 5 are higher and 9 lower than that defined for pure CO_2. These data indicate the presence of an additional component or components in the CO_2-rich fluid. The 5 higher temperatures are anomalous: while marginally outside the error range, they were reproducible, and are probably real. However, no common gaseous species miscible at low temperatures with CO_2 and associated with basaltic magmas is known to cause an increase in the solid-phase melting temperature.

Figure 3 is a histogram of all homogenization temperatures. Although the majority of inclusions homogenized to liquid, a few homogenized to vapor. Data from inclusions in which both melting temper-

Table 2. Low-T properties of magmatic vapor species

Species	Critical T, °C	Critical P, bars	Melting T, °C
CO_2	+31.1	73.6	-56.6
SO_2	+157.8	78.5	-72.7
H_2S	+100.4	89.8	-85.5
COS	+104.8	65.7	-138.2
CH_4	-82.1	46.3	-182.5
Ar	-122.3	48.5	-189.2
CO	-140.0	34.8	-199.0

Data from Weast (1974).

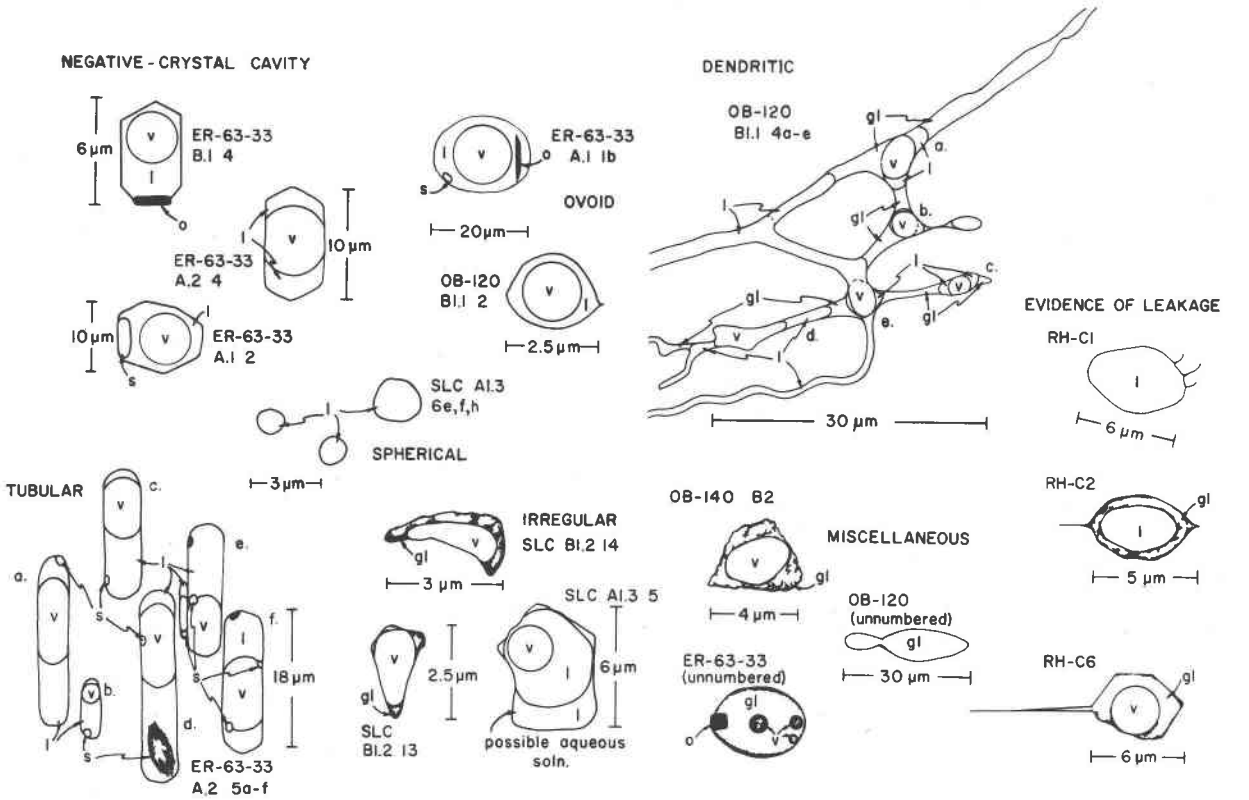

Fig. 1. Sizes and morphologies of representative inclusions in olivine and pyroxene. Sequences of letters and numbers are sample and inclusion identification. Abbreviations for labeled phases are: v, vapor; l, liquid; s, solid; o, opaque solid; gl, glass.

ature and homogenization temperature were determined are illustrated in Figure 4. More than 85 percent of these inclusions, virtually all of those from samples SLC, RH, and OB-120, fall within the defined range for pure CO_2.

Approximately 50 percent of the inclusions in sample ER-63-33 homogenize to liquid at temperatures above 31.1°C, and the melting temperature of most of these is below −56.6°C (Fig. 4). These observations indicate the presence of another component, miscible with liquid and gaseous CO_2, which has a higher critical temperature than pure CO_2 (31.1°C) and a melting temperature lower than pure CO_2 (−56.6°C). Of the stable species likely to occur in volcanic gases and miscible at cryogenic temperature with CO_2, those with critical temperatures higher than 31.1°C are SO_2, H_2S, and COS (Table 2). A small amount (on the order of 0.05 to 0.10 mole fraction) of any of these three components in a CO_2-rich fluid could account for the observed homogenization temperatures. Of these, the melting temperatures of SO_2 and H_2S are closer to that of CO_2, making them more likely than COS to be present in the inclusions.

We analyzed the glass linings (Fig. 1) of several inclusions from samples OB-120 and RH. The analyses (Table 4) were made with an automated energy-dispersive analysis system attached to an ARL-EMX microprobe; the technique is described in Hollister and Crawford (1977). The compositions (Table 4) clearly indicate the glasses were silicate melts, and therefore that the CO_2 fluids were associated with a melt when entrapped. The actual compositions of the originally entrapped melts can be approximated by mixing the compositions of the host-mineral, which may be presumed to have crystallized on the walls of the inclusions after entrapment, with the glass compositions. The most reasonable mixes give high-alumina andesite for 92 percent OB 120-2 glass plus 8 percent olivine (but the match is poor for MgO/FeO)

Table 3. Representative observations and calculations

Sample #	T_H,°C	dT/dt at T_H	T_M,°C	dT/dt at T_M	ρ,+	P,kbar, at 1200°C
ER-63-33	+36.0L	1.5				
	+32.0L	0.5	-57.1	0.3		
	+32.4L		-57.6	0.4		
	+31.1L-C	0.2	-56.3	0.2	0.47	2.2
	+29.9L	1.0	-56.4	0.1	0.59	3.0
	+32.1L	0.5	-56.7	0.2		
	+29.1L	1.0	-56.4	0.3	0.62	3.4
OB-i20	+30.9G-C	0.5	-56.2	0.1	0.38	1.4
	+24.3L	3.0	-55.9	0.2		
	+29.9G	0.5	-56.3	0.2	0.34	1.2
SLC	+30.1L	1.0			0.58	3.0
	-48.6L	1.0	-56.2	0.3	1.14	10.0
	+27.3L	0.5	-56.2	0.2	0.66	3.8
	+22.7L	0.2	-56.6	0.2	0.73	4.6
	+12.0L	1.0	-56.6**	0.2	0.84	6.0
	-36.9L	0.5	-56.6	0.3	1.10	9.4
RH	-18.8L	1.0	-56.2	0.3	1.02	8.3
	-23.8L	1.0			1.04	8.5
	+23.7L	1.0	-56.6	0.3	0.72	4.5
	-17.8L	1.0	-56.4	0.2	1.02	8.3
	-14.2L	1.5	-56.4	0.3	1.00	8.0

** with possible aqueous melting at higher T
+ only determined for pure CO_2 inclusions
* although elevated T_h are common in inclusions on this and other fracture surface, many of the inclusions are too small and dark for observation of melting phenomena.

Column headings: T_H, temperature of homogenization, L, to Liquid; G, to gas, L-C, to liquid as meniscus fades; G-C, to gas as meniscus fades. dT/dt at T_H, heating rate in °C/min at observed T_H; T_M, temperature of disappearance of solid CO_2 in presence of liquid and vapor (final melting temperature). dT/dt at T_M, heating rate at observed T_M. ρ, bulk density of pure CO_2 determined from T_H. P, kbar at 1200°C as determined from Figure 5.

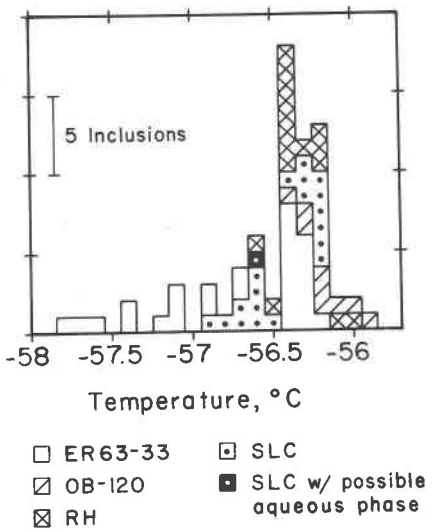

Fig. 2. Histogram of observed final melting temperatures of CO_2 solid coexisting with liquid and vapor and distinguished by sample number.

and high-alumina basalt for 75 percent RH-3 plus 25 percent clinopyroxene. The classification is from Irvine and Baragar (1971).

Discussion

The majority of inclusions appear to be pure CO_2. This allows the bulk density of fluid to be calculated

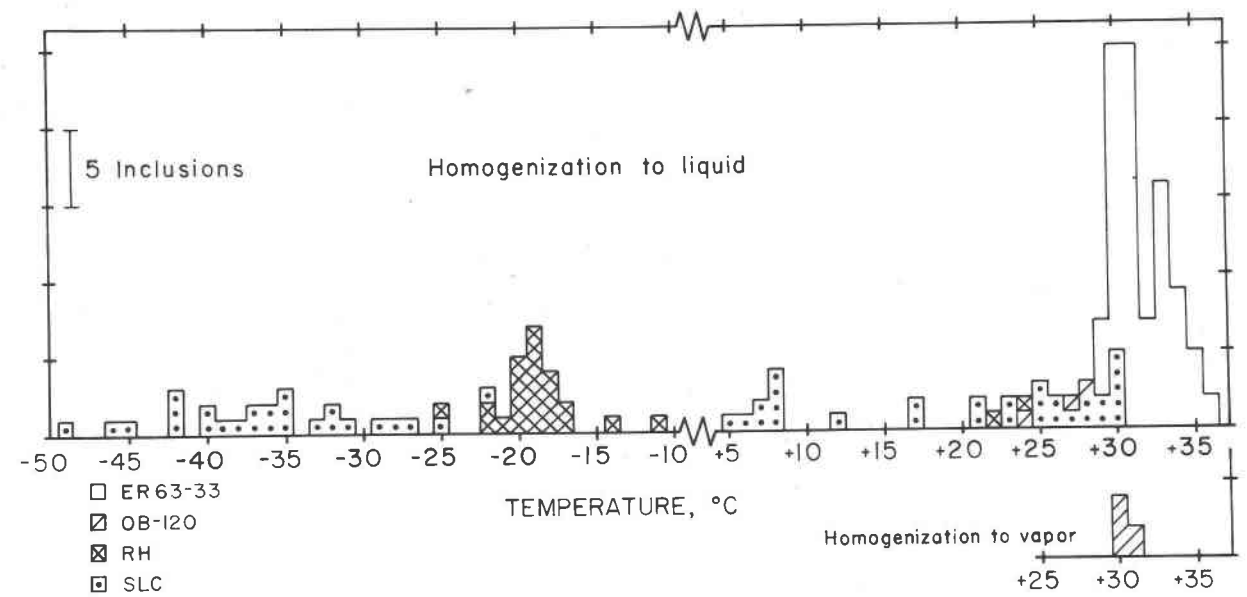

Fig. 3. Histogram of observed homogenization temperatures of individual inclusions distinguished by sample number. A small number of inclusions homogenize to vapor.

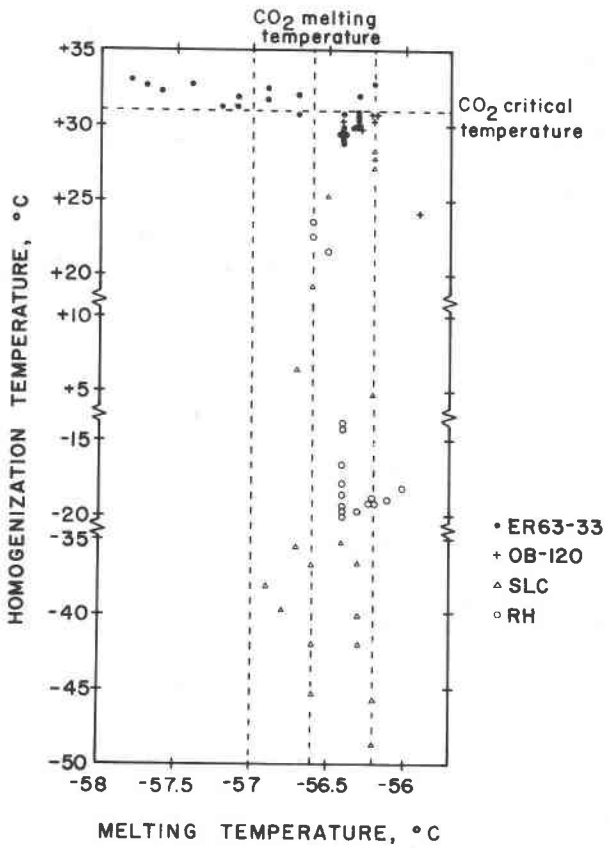

Fig. 4. Homogenization temperature *vs.* final melting temperature for individual inclusions from different samples. Note that some inclusions from sample ER-63-33 have homogenization temperatures *above* the critical temperature for CO_2 (31.1°C) *and* final melting temperatures *below* the pure CO_2 invariant temperature (−56.6°C).

from the observed homogenization temperature and the liquid- and vapor-saturated densities of pure CO_2 given by Newitt *et al.* (1956). These results are displayed as a histogram in the lower portion of Figure 5. The bulk densities of inclusions in each of the four samples have distinct and unique ranges. The apparently pure CO_2 inclusions in sample ER-63-33 have densities ranging from 0.45 to 0.62 gm/cm³; in sample OB-120, from 0.34 to 0.38 gm/cm³; in RH, from 0.72 to 1.04 gm/cm³; and in SLC, from 0.58 to 1.14 gm/cm³. These data can be combined with the experimentally determined P, ρ, T properties of pure CO_2 at high temperature to determine a pressure of entrapment, assuming a temperature of entrapment.

The upper portion of Figure 5 displays P–ρ isotherms for pure CO_2, based on readily available literature data to 1000°C and 10 kbar and extrapolated by us to 1200°C (see caption for references). Since these xenoliths were brought to the surface in lavas, we have assumed a maximum entrapment temperature of 1200°C for the CO_2 inclusions in the xenoliths. At this temperature the maximum observed densities of pure CO_2 inclusions define maximum entrapment pressures of 1.4 kbar for sample OB-120, 3.4 kbar for ER-63-33, 8.5 kbar for RH, and 10 kbar for SLC.

Furthermore, many of the inclusions from sample RH (maximum P = 8.5 kbar) appear to be "primary"; that is, they occur as isolated inclusions or in random groups rather than on fracture surfaces. This sample is therefore most likely to contain fluids actually entrapped at the time of formation of the xenolith. The majority of inclusions in the remaining samples, however, are definitely secondary; *i.e.*, they occur on healed fracture surfaces, and therefore define minimum constraints on the pressure and depth history of the sample.

Conclusions

Data and conclusions from this study are consistent with the previous observations of Roedder (1965). Precise melting and homogenization measurements confirm that most of the inclusions contain essentially pure CO_2. In one sample (ER-63-33), how-

Table 4. Analyses (oxide weight percent) of glass rims of inclusions

	OB 120			RH			
oxide	1	2	3	1	2	3	4
SiO_2	57.3	60.0	59.1	52.6	53.4	50.9	50.4
Al_2O_3	17.4	19.4	20.8	20.2	21.7	20.6	20.2
FeO*	3.9	2.7	2.9	6.1	7.7	11.1	10.3
MgO	12.3	6.6	3.9	3.4	2.0	3.0	3.8
CaO	6.1	7.1	8.5	6.5	4.8	6.6	7.3
Na_2O	3.3	3.8	4.6	5.3	4.0	4.9	5.1
K_2O	1.2	1.2	1.4	.3	1.9	1.6	1.6
TiO_2	0.3	0.6	0.6	1.5	1.1	1.3	1.4
P_2O_5	n.d.	n.d.	n.d.	.6	.4	.3	.2
Total	101.8	101.4	101.8	96.5	97.0	100.0	100.3

FeO/MgO: olivine host 0.15; Clinopyroxene host 0.32

*All Fe as FeO; n.d.-not determined

Analysis by the energy dispersive analysis system.

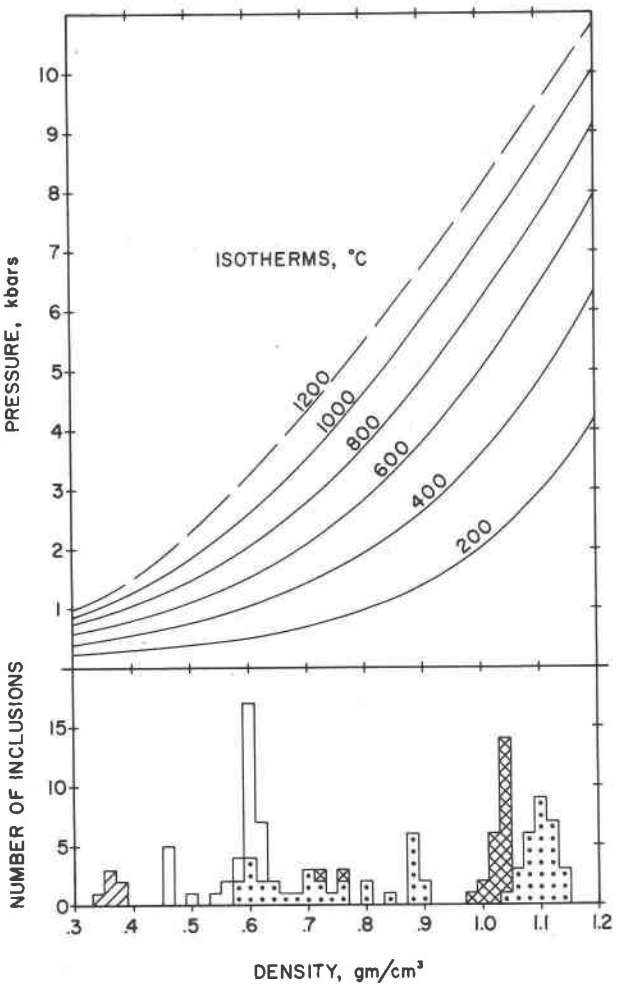

Fig. 5. Lower half is a histogram of densities of pure CO_2 inclusions calculated from the homogenization temperatures of individual inclusions in different samples. Symbols are the same as Figs. 1 and 2. Upper portion illustrates the isothermal P–ρ relations at several temperatures for pure CO_2 from the experimental work of Kennedy (1954), Juza *et al.* (1965), and Shmonov and Shmulovich (1974) to 10 kbar and 1000°C. The 1200°C isotherm is extrapolated. Note that the density scale for the histogram and P–ρ diagram is the same.

ever, there is a well-defined group of inclusions containing one or more added constituents, miscible with CO_2. SO_2 and/or H_2S, in concentrations of about 0.05 to 0.10 mole fraction of the fluid, are the most likely candidates for the additional components.

Densities of fluids in inclusions containing apparently pure CO_2 vary from 0.34 to 1.14 gm/cm³, implying minimum ambient pressures during final entrapment of as great as 10 kbar or more, assuming entrapment occurred at 1200°C.

The presence of glass, whose composition is approximately high-alumina andesite in OB-120 and high-alumina basalt in RH, as a constituent in some of the inclusions implies the coexistence at depth of CO_2, as the major volatile species, with a melt phase. The apparent lack of H_2O in the fluid inclusions indicates that any aqueous components were probably strongly partitioned into the melt phase.

Clearly, additional studies of fluid inclusions in ultramafic xenoliths, together with the compositions of the associated glass, would be an important contribution to the understanding of the role of volatile species in the lower crust and upper mantle.

Acknowledgments

We gratefully acknowledge Edwin Roedder for his help during the early stages of this research, and particularly for making available to us sample ER-63-33. Dale Jackson and Robert Hargraves criticized drafts of the manuscript, and we thank Fred Frey for his review of the final manuscript. Financial support was provided by NSF grant DES75-03259.

References

Christiansen, L. J. (1974) Phasengleichgewichtsprobleme bei der Abscheidung von H_2S, CO_2 und CO aus Erdgasgemischen. *Petrochem. ver. mit Brennstoff-Chem., 27,* 130–134.

Cummings, L. W. T. (1931) High-pressure rectification. I. Vapor-liquid equilibrium relations at high pressures. *Ind. Eng. Chem., 23,* 900–902.

Funkhouser, J. G. and J. J. Naughton (1968) Radiogenic helium and argon in ultramafic inclusions from Hawaii. *J. Geophys. Res., 73,* 4601–4607.

Gerlach, T. M. and B. E. Nordlie (1975) The C–O–H–S gaseous system Part I: Composition limits and trends in basaltic cases. Part II: Temperature, atomic composition, and molecular equilibria in volcanic gases. Part III: Magmatic gases compatible with oxides and sulfides in basaltic magmas. *Am. J. Sci., 275,* 353–410.

Hollister, L. S. and R. C. Burruss (1976) Phase equilibria in fluid inclusions from the Khtada Lake metamorphic complex. *Geochim. Cosmochim. Acta, 40,* 163–175.

——— and M. L. Crawford (1977) Melt immiscibility in Apollo 15 KREEP: origin of Fe-rich mare basalts. *Proc. 8th. Lunar Sci. Conf.*, in press.

Irvine, T. N. and W. R. A. Baragar (1971) A guide to the chemical classification of the common volcanic rocks. *Can. J. Earth Sci., 8,* 523–548.

Juza, J., V. Kmonicek and O. Sifner (1965) Measurements of the specific volume of CO_2 in the range of 700 to 4000 b and 50° to 475°C. *Physica, 31,* 1735–1744.

Kennedy, G. C. (1954) Pressure–volume–temperature relations in CO_2 at elevated temperatures and pressures. *Am. J. Sci., 252,* 225–241.

MacDonald, G. A. and T. Katsura (1964) Chemical composition of Hawaiian lavas. *J. Petrol., 5,* #1, 82–133.

Murck, B. (1976) *A Study of Fluid Inclusions in Ultramafic Rocks.* Senior thesis, Princeton University, Princeton, New Jersey.

Newitt, D. M., M. U. Pai, N. R. Kuloor, and J. A. W. Hugill (1956) Carbon dioxide. In F. Din, Ed., *Thermodynamic Func-*

tions of Gases, Vol. 1, p. 102–134. Butterworth's Scientific Publications, London.

Poty, B., J. Leroy and L. Jachimowitz (1976) Un nouvel appareil pour la measure des temperatures sous le microscope: l'installation de microthermometrie Chaixmeca. *Bull. Soc. fr. Mineral. Cristallogr., 99,* 182–186.

Rama, S. M. I., S. R. Hart and E. Roedder (1965) Excess radiogenic argon in fluid inclusions. *J. Geophys. Res., 70,* 509–511.

Roedder, E. (1965) Liquid CO_2 inclusions in olivine-bearing nodules and phenocrysts from basalts. *Am. Mineral., 50,* 1746–1782.

Shmonov, V. M. and K. I. Shmulovich (1974) Molar volumes and equation of state of CO_2 at temperatures from 100° to 1000°C and pressures from 2000 to 10,000 bars. (trans.) *Dokl. Acad. Sci. USSR, 217,* 206–209.

Sobocinski, D. P. and F. Kurata (1959) Heterogeneous phase equilibria of the hydrogen sulfide–carbon dioxide system. *Am. Inst. Chem. Eng. J., 5,* 545–551.

Weast, R. C., Ed. (1974) *Handbook of Chemistry and Physics,* 55th ed. CRC Press, Inc.

Manuscript received, May 9, 1977; accepted for publication, September 12, 1977.